Surface & Coatings Technology 355 (2018) 50–54

Contents lists available at ScienceDirect

Surface & Coatings Technology

journal homepage: www.elsevier.com/locate/surfcoat

Electrical characterization of molybdenum oxide lamellar crystals irradiated with UV light and proton beams

D.R. Pereira[a,b,d], M. Peres[a], L.C. Alves[b], J.G. Correia[b], C. Díaz-Guerra[c], A.G. Silva[d], E. Alves[a], K. Lorenz[a,*]

[a] IPFN, Instituto Superior Técnico, Universidade de Lisboa, Estrada Nacional 10, km 139.7, 2695-066 Bobadela LRS, Portugal
[b] C2TN, Instituto Superior Técnico (IST), Campus Tecnológico e Nuclear, Estrada Nacional 10, km 139.7, 2695-066 Bobadela LRS, Portugal
[c] Departamento de Física de Materiales, Facultad de Ciencias Físicas, Universidad Complutense de Madrid, Madrid, Spain
[d] Departamento de Física, Faculdade de Ciências e Tecnologia, Universidade Nova de Lisboa, Campus da Caparica, 2829-516, Caparica, Portugal

ARTICLE INFO

Keywords:
Molybdenum trioxide
Ion beam induced conductivity
Photoconductivity

ABSTRACT

MoO_3 lamellar single crystals were processed into planar metal-semiconductor-metal devices and subjected to irradiation cycles with ultraviolet light and 2 MeV protons in vacuum. In-situ electrical characterization demonstrates that these sensor devices respond well to the radiation with a gain of ~30% upon proton irradiation. However, response times are slow and strong persistent photoconductivity and ion beam induced conductivity are observed when the excitation source is switched off. The current decay is strongly increased when the irradiation chamber is vented with air suggesting that surface processes are at the origin of persistent conductivity. The observed conductivity changes are explained based on a model considering the creation of electron-hole pairs as well as adsorption and desorption processes of oxygen molecules at the surface of the samples.

1. Introduction

Molybdenum trioxide, MoO_3, is a wide band gap semiconductor with an orthorhombic crystal structure in its most stable phase at room temperature. This phase has an anisotropic layered structure parallel to the (010) planes, that has been attracting increasing attention for multiple applications such as solar cells [1], gas sensors [2] and lithium ion batteries [3]. The concentration of oxygen vacancies and impurities in samples of MoO_3 has proved to be an important factor determining the electrical and optical properties of the material, since these defects create intermediate states within the band gap, which may affect the electrical conductivity and electron-hole recombination processes. In particular, oxygen vacancies can be introduced in two distinct ways: during the growth process by controlling parameters such as the growth temperature and partial pressure of oxygen and, after growth, e.g. by annealing treatments under low partial pressures of oxygen or in reducing atmosphere [4]. A correlation between the increase in conductivity and the creation of oxygen vacancies was observed in MoO_3 nanobelts annealed in a reducing hydrogen atmosphere. It is found that oxygen vacancies act as donors that can provide electrons to the conduction band at room temperature [5]. In addition, the growth conditions also influence the morphology of the samples and their phase purity [6, 7]. The influence of stoichiometry on the electrical conductivity of MoO_x is demonstrated by the semiconducting behaviour of the MoO_x phases ($2 < x \leq 3$) and the metallic behaviour of the MoO_2 phase [7].

Wide band gap oxide semiconductors such as TiO_2 and ZnO, are promising materials for ultraviolet (UV) sensors [8–12]. Also ions can be readily detected by simple metal-semiconductor-metal devices [13]. D. Xiang et al. [5], showed that MoO_3 nanobelts, annealed in a hydrogen-reducing atmosphere, exhibited not only high electrical conductivity but also a high response as a radiation sensor in the visible spectral region. In-situ ultraviolet photoelectron spectroscopy (UPS) and X-ray photoelectron spectroscopy (XPS) revealed that these changes are due to the creation of intermediate states within the band gap resulting from the different oxidation states of the Mo present in MoO_3 [5]. MoO_3 nanosheets were furthermore shown to be promising material for flexible UV detectors [14].

In this work, MoO_3 planar metal-semiconductor-metal devices were processed and tested as sensors for UV and proton radiation.

2. Experimental details

The samples of molybdenum oxide lamellar crystals used in this work were grown by an evaporation-solidification method. Mo powder (~700 mg) was compacted under a compressive load of two tons to

* Corresponding author.
E-mail address: Lorenz@ctn.tecnico.ulisboa.pt (K. Lorenz).

https://doi.org/10.1016/j.surfcoat.2018.01.034
Received 31 October 2017; Received in revised form 9 January 2018; Accepted 10 January 2018
Available online 11 January 2018
0257-8972/

form a disc with 7 mm diameter and 2 mm thickness. The particle size of the Mo powder varies between 1 and 5 μm. The disc was then placed in a horizontal, cylindrical, tube furnace with 20 cm length and 8 cm radius using a quartz tube of 28 cm length and 2.2 cm diameter. The precursor disc is placed at the centre of the furnace, where the temperature is maximum, and heated to a temperature of 750 °C during 10 h in an air flow of 2 l/min using compressed air. No prior vacuum was established in the quartz tube; hence, some water vapour may be present in the growth ambient. The temperature does not significantly differ from the set-value in a length interval of about 4 cm around the centre of the furnace, but progressively decreases towards the ends of the furnace. The lamellar crystals were deposited at the cooler zones of the tube where the temperature is about 400–450 °C. After the growth run finishes, the Mo disc is no longer observed; hence, the metal precursor reacts completely.

Scanning electron microscopy and atomic force microscopy images show that the thickness of the as-grown samples varies between 100 nm and 10 μm, but most of them (approximately 70%) have thicknesses in the (2–4) μm range and lateral dimensions of about $2 \times 5\,mm^2$ [15]. Samples are very brittle and cleave easily parallel to the surface leading to inhomogeneous sample thickness. X-ray diffraction measurements confirmed the single crystalline growth of the orthorhombic α-MoO_3 phase with (010) surface orientation of the crystals. Since as-grown samples showed a very high electrical resistivity, leading to very noisy I-V curves that were not modified by UV or proton irradiation, the samples were annealed in vacuum (approximately 1×10^{-4} mbar) at 300 °C for 30 min. Annealing was performed in an ANNEALSYS halogen lamp furnace where the samples were placed between two pieces of silicon. Upon annealing a significant increase in the electrical conductivity was achieved, with currents increasing from the nano-Ampère to the micro-Ampère range, attributed to the creation of oxygen vacancies. The preferential loss of O during annealing in oxygen poor environment accompanied by an increase of conductivity has been reported before [16]; however, the reduction of MoO_3 due to intercalated hydrogen, ultimately also leading to the formation of oxygen vacancies, may also play a role in the observed conductivity increase [17]. Preliminary UV Raman measurements on vacuum annealed samples (not shown) only show bands characteristic of α-MoO_3. Furthermore, they reveal a broadening of the Raman bands centered at 819 and 996 cm^{-1} and the intensity ratio of the Raman bands at 283 and 291 cm^{-1} (I_{283}/I_{291}) decreases after annealing which are typical signs for the formation of oxygen vacancies [7]. No colour change has been observed at the temperature used in the present study.

The metal-semiconductor-metal (MSM) devices were fabricated using a glass substrate, an as-annealed sample and two co-planar indium contacts. The indium contacts were applied by placing two stripes of In on top of the sample with a distance of about 2 mm between them and then heating the sample to ~150 °C. After the In melted, the structure was cooled down and the contacts solidified. The lateral MSM geometry was chosen because of the easy device processing and the possibility to use the same device for UV light and particle detection e.g. without using transparent contacts. In III-nitride photodetectors, high quantum efficiency was demonstrated for devices with MSM configuration [18]. This configuration also allows the proton irradiation of MoO_3 in between the contacts, avoiding any change of the In/semiconductor interface due to the irradiation.

Electrical measurements were performed using an Agilent B1500A Semiconductor Device Analyser. I-V curves were taken at ambient pressure before and after the irradiation with UV light and protons. Transient I-t measurements during irradiations were carried out in vacuum applying a 10 V bias to the device. The same device was first exposed to UV radiation and several days later to 2 MeV protons. Both photoconductivity and ion beam induced conductivity measurements were performed inside vacuum chambers with a pressure of about 5×10^{-5} mbar. Keeping the sample at this pressure during several days does not lead to significant changes of the conductivity, in contrast to samples kept in air which suffer a strong decrease of the conductivity on a timescale of days, indicating that the effect of residual gases in the chamber are negligible for the observations during irradiation presented here.

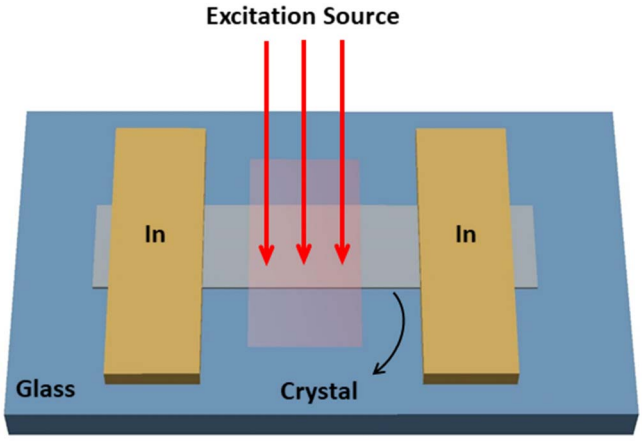

Fig. 1. Schematic illustration of a MoO_3 lamellar crystal device for photoconductivity and ion beam induced conductivity measurements.

A scheme of the device and measurement geometry for photoconductivity and ion beam induced conductivity measurements is shown in Fig. 1. For the photoconductivity measurements, the device was excited with the entire spectrum of a deuterium lamp (Hamamatsu High Power UV–Vis Fiber Light Source L10290) that emits in the range of 200 nm to 400 nm. Proton irradiation was performed at the IST/LATR microprobe [19] using a 2 MeV proton beam with a current of 500 pA. Approximately 75% of the area of the device between the contacts (the contacts themselves were not hit by the proton beam) was irradiated with a proton flux of $\sim 2 \times 10^{11}$ particles·cm^{-2}·s^{-1}. The projected range of 2 MeV protons in MoO_3 (approx. 30 μm according to SRIM simulations [20]) is larger than the typical sample thickness (< 10 μm) so that most protons will exit the sample at the back side and energy deposition occurs mainly via electronic interactions (creation of electron-hole pairs) while defect formation via nuclear collisions remains low. Such a device structure may be interesting for dosimetry purposes (measuring the intensity of the irradiation but not the energy of the particles) or as a trigger to detect particles before they are implanted in a material below the device e.g. for single ion implantation. In the present case, these irradiation conditions allow a more direct comparison between the device behaviour upon UV and proton irradiation since atomic displacements upon particle irradiation are suppressed.

3. Results and discussion

Fig. 2 summarizes the results of the I-V and transient I-t electrical characterization. The I-V curves taken in air before and after irradiation with UV light and protons (Fig. 2.a and c, respectively) present nearly linear characteristics suggesting contacts with quasi ohmic character. Furthermore, no significant changes are observed in the I-V curves after UV or proton irradiation suggesting that irreversible structural changes, induced during the irradiation, are negligible.

The slight decrease of the conductivity seen when comparing Fig. 2.a (showing I-V curves in the dark before and after the photoconductivity measurements) and Fig. 2.c (showing I-V curves in the dark taken several days later just before and after the ion beam induced conductivity measurements) is attributed to the adsorption of oxygen molecules at the surface occurring during storage of the sample in the vacuum chamber for several days. Note that the conductivity of annealed MoO_3 samples decreases strongly with time, on a timescale of days, if samples are left in air ambient. This is attributed to oxygen

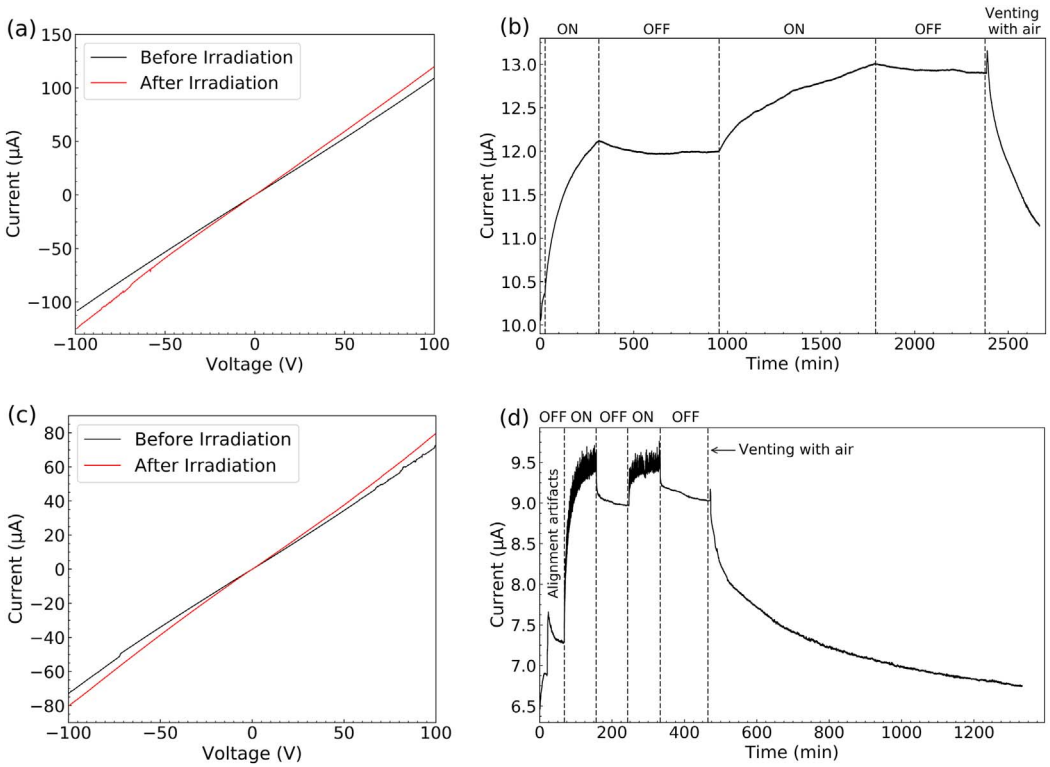

Fig. 2. (a): I-V curves of the device before and after photoconductivity measurements. (b): Response of the device during exposure to UV radiation cycles with an applied voltage of 10 V. (c): I-V curves of the device before and after ion beam induced conductivity measurements. (d): Response of the device during exposure to proton irradiation cycles with applied voltage of 10 V.

adsorption at the surface; this effect will be discussed in detail below.

Fig. 2.b shows the response of the device when exposed to UV radiation in vacuum. An increase of the conductivity is clearly seen when irradiation is switched on. The current value increases first more sharply in the first few minutes, followed by a slower increase over the remaining measurement time. During the first irradiation cycle of 280 min, the current value increases by approximately 18% but never reaches steady state saturation. When the UV light source is switched off, the current decreases very slowly and stabilizes only 1% below the value before the light was switched off. In the second irradiation cycle the current increases again first rapidly and then slowly to values well above the values reached in the first cycle and again without reaching saturation. The decrease of current after switching off the UV lamp is negligible revealing extreme persistent conductivity. At time t = ~2380 min, the chamber was vented with air leading to an abrupt decrease of the current in the first minutes, followed by a more gradual decrease to a value close to the initial one (see Fig. 2.a).

The ion beam induced conductivity measurement is shown in Fig. 2.d. Similar to the photoconductivity results, when the device is exposed to the proton beam, the current value increases first rapidly and then more slowly. In contrast to the photoconductivity measurements, the current saturates after approximately 75 min of proton irradiation reaching a gain of 31%. When the proton beam is switched off, the current first drops rapidly and then more slowly saturating at a value approximately 5% below the value before the beam was switched off. If a second irradiation cycle is performed, the device exhibits similar behaviour, i.e. the current increases/decreases initially more rapidly followed by a period in which the increase/decrease occurs at a lower rate, when the source is turned on/off. The current stabilizes at the same level as during the first irradiation, in contrast to the photoconductivity experiment. Again the current level decreases rapidly when the chamber is placed at atmospheric pressure and it reaches the same level as before the proton irradiation (see Fig. 2.c).

The main difference between photo- and ion beam induced conductivity is the fact that both current increase and decrease take place at a faster rate for the case of proton irradiation. Although the difference in the current vs. time ascents for UV and proton excitation may be influenced by the different excitation densities, the significant discrepancy in the decay times suggests that the behaviour is dominated by different processes. In particular, the fast decrease of the current when the excitation source is switched off is more accentuated for proton irradiation. Such differences may be related to the depth of penetration of the protons in comparison to the UV radiation, i.e., as the protons have a range of approximately 30 μm, the processes of creating electron-hole pairs occur in the entire cross section of the sample, while with UV radiation most of the light is absorbed close to the surface. Such behaviour suggests that the persistent conductivity seen in both experiments is probably due to processes occurring at the surface, whereas the processes occurring in the bulk (preferentially induced by the more penetrating protons) contribute mainly to the abrupt variation of the current. As will be discussed below, surface effects, such as adsorption and desorption of molecules, are much slower than simple electron-hole formation and recombination. This reasoning is also supported by the strong decrease in the conductivity after venting any of the experimental irradiation chambers used.

For both irradiation types, when the external stimuli is switched off the conductivity stabilizes at much higher level than the initial value of the current (before the excitation source was switched on for the first time). This persistent current is particularly strong for the case of photoconductivity. Furthermore, in both experiments the conductivity recovers its initial low value when the device is placed at atmospheric conditions. This reveals the importance of the atmosphere in the response of the device and thus the role of surface effects.

Similar responses and persistent conductivity have been reported for ZnO nanowires exposed to UV radiation in different atmospheres, in particular, showing a faster current decay for oxygen containing environments [21, 22]. The strong influence of the atmosphere on the photoconductivity was attributed to adsorption and desorption

processes of oxygen molecules at the surface, which allowed not only to explain the variations along a cycle but also the differences observed in the responses obtained in vacuum and air [22]. It is assumed that the adsorption of O_2 is the dominant process leading to the decay of conductivity observed here since adsorbed O_2 will accept electrons from the n-type oxide semiconductor forming O_2^-. Adsorption of water molecules on the other hand leads to an increase of conductivity in MoO_3 [23].

Based on the similar results for ZnO and MoO_3, in the following, we adapt the model of persistent photoconductivity developed for ZnO to MoO_3. First, we need to note that unlike ZnO, which is usually highly n-type doped, our as-grown MoO_3 crystals are insulating.

In fact, unannealed and freshly exfoliated samples have very high resistivity making I-V curve measurements impossible. Annealing in vacuum leads to the creation of oxygen vacancies, which increase the concentration of free carriers (electrons). This assumption is in agreement with the strong conductivity increase measured in our samples after annealing and with results found in the literature [5, 7, 24] and it is supported by our preliminary Raman measurements described in the previous section.

According to the model explaining persistent current in oxide semiconductors, electrons in the conduction band can migrate easily to the surface, where they can be trapped by oxygen molecules that are close to the surface of the sample, which favours the oxygen adsorption processes. Due to the trapping of free carriers from the conduction band, the conductivity is reduced and oxygen adsorption will determine the initial conductivity of the device (which will be lower than expected taking into account the donor (oxygen vacancy) concentration). At the same time, electron trapping at the surface increases the concentration of negative charges in this region, resulting in an increased band bending when the concentration of adsorbed molecules increases – see Fig. 3.a.

This band bending can cause an increase of the lifetime of irradiation induced electrons in the conduction band, due to fast separation of the generated electron-hole pairs. This rise in the lifetime of the electrons increases the photoconductivity and ion beam induced conductivity gains, while preventing the quick recovery of the initial current value after the excitation source is switched off.

When the devices are exposed to UV radiation or to protons, a rapid increase in the current value is initially verified, which may be related to the rapid creation of electron-hole pairs. Due to band bending, the generated holes will migrate to the surface of the sample where they can recombine with electrons captured by adsorbed oxygen molecules, causing desorption of the molecules – see Fig. 3.b. This will decrease the band bending and promote the recombination of carriers. Since the process of desorption of oxygen molecules from the surface is a slower process than the generation and separation of electron-hole pairs, the increase of the current value will also become slower. As the measurements were done in vacuum, this slow increase can continue until reaching a level corresponding to that expected for a crystal with the same concentration of donors but without capture of the electrons at the surface (i.e. all oxygen molecules are desorbed) [22].

In the case of ZnO, some authors have also attributed an increase in current to higher than expected values, even for a crystal without oxygen molecules adsorbed on the surface, to the desorption of elemental oxygen from the crystal lattice, which occurs at a slower rate than desorption of the oxygen molecules [21].

As mentioned, desorption of oxygen molecules from the surface causes a decrease in the band bending, which favours the migration of electrons to the surface and consequently the re-adsorption of oxygen molecules. After some time, an equilibrium between these two processes can be reached (at a level depending on the oxygen concentration in the sample environment) leading to a current saturation – see Fig. 3.b.

In the photoconductivity measurement – Fig. 2.b - the current value does not reach a saturation level, which may mean that the equilibrium between adsorption and desorption processes of oxygen molecules on the surface has not been reached during the measurement. In the case of the ion beam induced conductivity measurement – Fig. 2.d - a saturation of the current value is verified, which may result from a higher

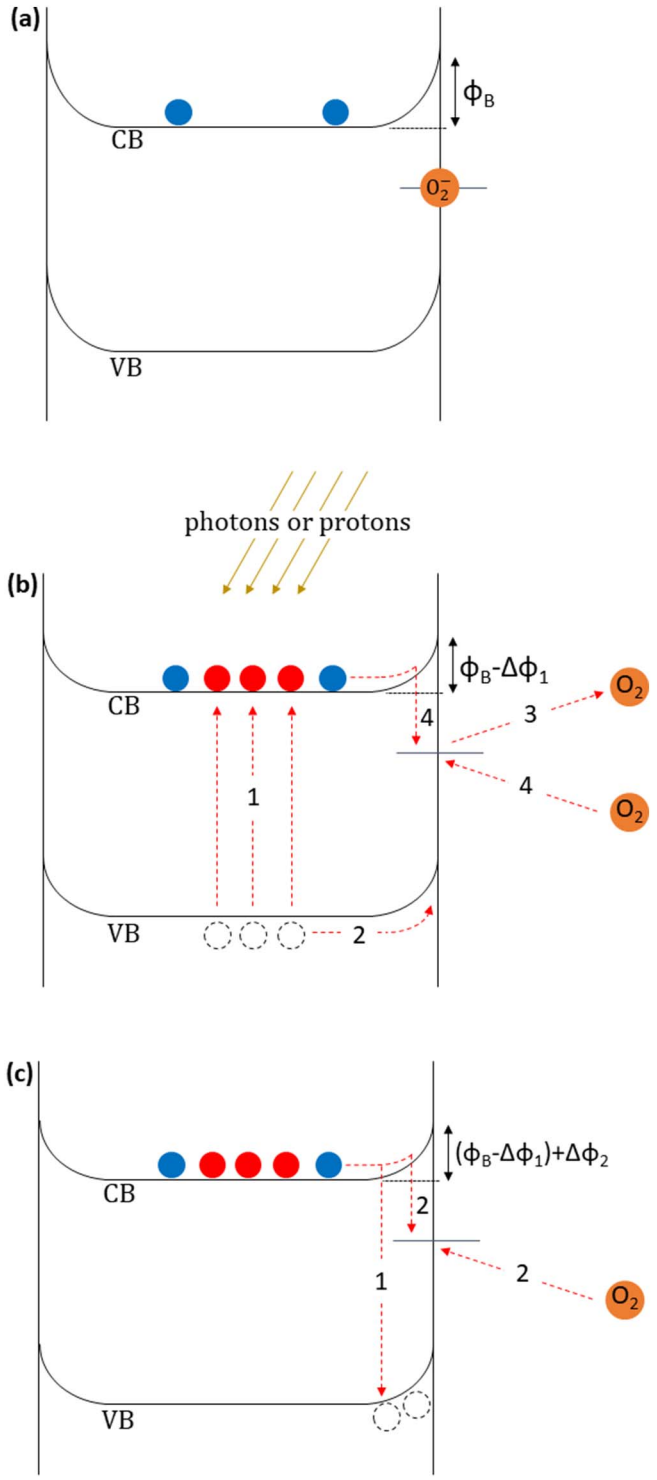

Fig. 3. Schematic of the processes involved in the persistent photoconductivity and ion beam induced conductivity in as-annealed samples of MoO_3: (a) before, (b) during and, (c) after the irradiation process. Red and dotted circles symbolize electrons and holes created by irradiation, respectively, while blue circles represent the free electrons resulting from the annealing process. The numbers in (b) and (c) indicate the order in which the processes occur. Adapted from [22]. VB: valence band; CB: conduction band. (For interpretation of the references to colour in this figure legend, the reader is referred to the web version of this article.)

excitation density compared to the photoconductivity test leading to faster oxygen desorption.

When the excitation source is switched off, a rapid recombination of electron-hole pairs can lead to a fast decrease in the current value followed by the re-adsorption of oxygen molecules at the surface which reduces the current but at a slower pace – see Fig. 3.c. A continuous pumping of oxygen molecules to the outside of the chamber does not favour the re-adsorption processes, leading to a stabilization of the current at a much higher level than the initial value, remaining there for hours. Thus, the fast decrease in the current value in the first minutes after switching off the excitation is essentially due to the recombination of electrons in the conduction band with holes that exist in the valence band, followed by a slow and almost non-existent decrease of the current when there are no holes available in the valence band.

When the chamber is vented with air, there is a more pronounced decrease in the current to values close to the initial one, which is attributed to the presence of oxygen molecules inside the chamber. As the concentration of oxygen molecules near the surface of the device increases abruptly immediately after the chamber is opened, the capture of electrons by oxygen molecules can occur quickly, which causes a more abrupt decrease of the current value. However, such electron capture will cause a bending of the bands at the surface, which makes it more difficult for the electrons to migrate to the surface, thereby reducing the rate of adsorption of oxygen molecules. This results in a more gradual decrease of the current, as is observed in both measurements.

It is also worth mentioning that in the first instants when venting the chamber, there is a significant increase in the value of the measured current. On the other hand, a sharp current decrease was observed in the first pumping moments during the lowering of the pressure inside the chamber. These observations suggest that this type of material has a response to pressure variations, and that in the future it can be studied for pressure variation sensors.

Finally, it is worth to emphasize that, as shown in Fig. 2.c, the characteristic I-V curve of the device did not undergo any significant changes during the proton irradiation to an overall fluence of approximately 1.8×10^{15} particles·cm^{-2}, revealing excellent radiation resistance of MoO_3.

4. Conclusions

In this work, we investigated the response of the same device containing an annealed MoO_3 crystal when exposed to UV radiation and to a proton beam. Both photoconductivity and ion beam induced conductivity measurements revealed that the device is sensitive to both types of radiation albeit with long response and recovery times. The strong influence of the atmosphere on the conductivity of the device during the measurements but also during the storage of the samples suggests that the surface plays an important role determining the electrical properties of the samples. Both long response times and strong persistent conductivity are well described by a model considering the adsorption and desorption of oxygen molecules at the surface.

The conductivity under irradiation first increases quickly attributed to the creation of electron-hole pairs followed by their separation due to band bending. Then desorption of surface oxygen causes a slower increase of the current value which stabilizes when an equilibrium between desorption and re-adsorption of oxygen is reached.

After switching the excitation source off, strong persistent conductivity is observed. In vacuum the current stabilizes at a level much higher than the initial value before the irradiation and remains high for hours. When the device is placed at atmospheric pressure, the current value approached the initial value more rapidly attributed to the abrupt increase of oxygen molecules at the surface of the sample.

Proton irradiation did not lead to any irreversible changes in the I-V curves revealing high radiation resistance of MoO_3.

Acknowledgements

This work was supported by the Fundação para a Ciência e a Tecnologia (FCT) [grants CERN/FIS/NUC/0004/2015, UID/FIS/50010/2013, UID/Multi/04349/2013, SFRH/BPD/111285/2015 and Investigador FCT].

References

[1] H.-Y. Chen, et al., Indium-doped molybdenum oxide as a new p-type transparent conductive oxide, J. Mater. Chem. 21 (15) (2011) 5745–5752.
[2] S. Bai, et al., Intrinsic characteristic and mechanism in enhancing H_2S sensing of Cd-doped α-MoO_3 nanobelts, Sensors Actuators B Chem. 204 (2014) 754–762.
[3] X. Hu, W. Zhang, X. Liu, Y. Mei, Y. Huang, Nanostructured Mo-based electrode materials for electrochemical energy storage, Chem. Soc. Rev. 44 (8) (2015) 2376–2404.
[4] H.-S. Kim, et al., Oxygen vacancies enhance pseudocapacitive charge storage properties of MoO_{3-x}, Nat. Mater. 16 (4) (2017) 454–460.
[5] D. Xiang, C. Han, J. Zhang, W. Chen, Gap states assisted MoO_3 nanobelt photodetector with wide spectrum response, Sci. Rep. 4 (2014) 4891.
[6] M. Dieterle, G. Mestl, Raman spectroscopy of molybdenum oxides, Phys. Chem. Chem. Phys. 4 (5) (2002) 822–826.
[7] M. Dieterle, G. Weinberg, G. Mestl, Raman spectroscopy of molybdenum oxides, Phys. Chem. Chem. Phys. 4 (5) (2002) 812–821.
[8] H. Xue, et al., TiO_2 based metal-semiconductor-metal ultraviolet photodetectors, Appl. Phys. Lett. 90 (20) (2007) 1–4.
[9] C. Soci, et al., ZnO nanowire UV photodetectors with high internal gain, Nano Lett. 7 (4) (2007) 1003–1009.
[10] H. Kind, H. Yan, B. Messer, M. Law, P. Yang, Nanowire ultraviolet photodetectors and optical switches, Adv. Mater. 14 (2) (2002) 158–160.
[11] S.P. Ghosh, et al., Ultraviolet photodetection characteristics of zinc oxide thin films and nanostructures, Mater. Sci. Eng. 115 (2016) 12035.
[12] J. Zou, Q. Zhang, K. Huang, N. Marzari, Ultraviolet photodetectors based on anodic TiO_2 nanotube arrays, J. Phys. Chem. C 114 (24) (2010) 10725–10729.
[13] A. Johannes, R. Niepelt, M. Gnauck, C. Ronning, Persistent ion beam induced conductivity in zinc oxide nanowires, Appl. Phys. Lett. 99 (25) (2011) 252105.
[14] Q. Zheng, J. Huang, S. Cao, H. Gao, A flexible ultraviolet photodetector based on single crystalline MoO_3 nanosheets, J. Mater. Chem. C 3 (28) (2015) 7469–7475.
[15] M. Vila, C. Díaz-Guerra, D. Jerez, K. Lorenz, J. Piqueras, E. Alves, Intense luminescence emission from rare-earth-doped MoO_3 nanoplates and lamellar crystals for optoelectronic, J. Phys. D. Appl. Phys. 47 (35) (2014) 355105.
[16] S.-Y. Lin, Y.-C. Chen, C.-M. Wang, P.-T. Hsieh, S.-C. Shih, Post-annealing effect upon optical properties of electron beam evaporated molybdenum oxide thin films, Appl. Surf. Sci. 255 (6) (2009) 3868–3874.
[17] A. Borgschulte, O. Sambalova, R. Delmelle, S. Jenatsch, R. Hany, F. Nüesch, Hydrogen reduction of molybdenum oxide at room temperature, Sci. Rep. 7 (2017) 40761.
[18] L. Sang, M. Liao, M. Sumiya, A comprehensive review of semiconductor ultraviolet photodetectors: from thin film to one-dimensional nanostructures, Sensors 13 (8) (2013) 10482–10518.
[19] L.C. Alves, et al., Micron-scale analysis of SiC/SiCf composites using the new Lisbon nuclear microprobe, Nucl. Instrum. Methods Phys. Res. B 161–163 (2000) 334–338.
[20] J.F. Ziegler, J.P. Biersack, U. Littmark, The Stopping and Range of Ions in Solids, Pergamon, New York, 1985.
[21] J. Bao, et al., Photoinduced oxygen release and persistent photoconductivity in ZnO nanowires, Nanoscale Res. Lett. 6 (2011) 404.
[22] D. Cammi, C. Ronning, Persistent photoconductivity in ZnO nanowires in different atmospheres, Adv. Condens. Matter Phys. 2014 (2014) 184120.
[23] L. Khandare, S.S. Terdale, D.J. Late, Ultra-fast α-MoO_3 nanorod-based humidity sensor, Adv. Device Mater. 2 (2) (2016) 15–22.
[24] M. Madel, et al., Persistent photoconductivity in ZnO nanowires: influence of oxygen and argon ambient, J. Appl. Phys. 121 (12) (2017) 124301.